Journal of Alloys and Compounds 511 (2012) 176–188

Contents lists available at SciVerse ScienceDirect

Journal of Alloys and Compounds

journal homepage: www.elsevier.com/locate/jallcom

# Intermetallic compound growth suppression at high temperature in SAC solders with Zn addition on Cu and Ni–P substrates

H.R. Kotadia[a,*], O. Mokhtari[a], M.P. Clode[b], M.A. Green[a], S.H. Mannan[a]

[a] Department of Physics, King's College London, Strand, London WC2R 2LS, UK
[b] Materials Research Group, Division of Engineering, King's College London, London WC2R 2LS, UK

ARTICLE INFO

*Article history:*
Received 14 July 2011
Received in revised form 7 September 2011
Accepted 8 September 2011
Available online 16 September 2011

*Keywords:*
Soldering
Lead-free solder
Intermetallic compounds
Sn–Ag–Cu alloys

ABSTRACT

The effect of adding 0.5–1.5 wt.% Zn to Sn–3.8Ag–0.7Cu (SAC) solder alloy during reflow and solid state ageing has been investigated. In particular, the role of the Zn addition in suppressing interfacial Intermetallic Compound (IMC) growth on Cu and Ni–P substrates has been determined. Solder–substrate couples were aged at 150 °C and 185 °C for 1000 h. In the case of 0.5–1.0 wt.% Zn on Cu substrate, $Cu_3Sn$ IMC was significantly suppressed and the morphology of $Cu_6Sn_5$ grains was changed, leading to suppressed $Cu_6Sn_5$ growth. In the SAC–1.5Zn/Cu substrate system a $Cu_5Zn_8$ IMC layer nucleated at the interface followed by massive spalling of the layer into the solder, forming a barrier layer limiting $Cu_6Sn_5$ growth. On Ni–P substrates the $(Cu,Ni)_6Sn_5$ IMC growth rate was suppressed, the lowest growth rate being found in the SAC–1.5Zn/Ni–P system. In all cases the added Zn segregated to the interfacial IMCs so that $Cu_6Sn_5$ became $(Cu,Zn)_6Sn_5$ and $(Cu,Ni)_6Sn_5$ became $(Ni,Cu,Zn)_6Sn_5$. The effect of Zn concentration on undercooling, wetting angles and IMC composition changes during ageing are also tabulated, and a method of incorporating Zn into the solder during reflow without compromising solder paste reflow described.



## 1. Introduction

Interfacial reactions occur readily when a molten metal is in contact with a compatible solid metal (substrate). Such reactions involve interdiffusion between the liquid and solid metals and often result in the formation and growth of intermetallic compounds (IMCs) at the interface [1]. In this context, Pb–Sn alloys have been extensively studied and used for electronic interconnects. However, medical studies have shown that Pb is a heavy metal toxin that can damage the kidney, liver, blood, and the central nervous system [2]. Therefore, implementation of Sn-rich Pb-free solder manufacturing has become increasingly important in recent years due to the legislation to prohibit Pb in electronics products. Over the past two decades, considerable research has been carried out on Pb-free solders such as eutectic Sn–3.5Ag, Sn–0.7Cu, $Sn_xAg_yCu_z$ (SAC) and the IMCs formed with different substrates such as Cu, Ni, Ni–P during liquid and solid-state reaction [3–7]. From all these Sn-rich Pb-free solders, the SAC solder alloy has been identified as a promising candidate for electronics packages. However, many problems have been reported in SAC solder such as void formation in interfacial IMCs, higher IMC growth rates, spalling of interfacial IMCs during high temperature storage and large undercooling during solidification [8]. The problems become acute for high temperature applications when IMC growth rates accelerate.

During operation, electronic packages are usually subjected to a wide range of temperatures, especially in automotive, aerospace and traction industry applications. These components may experience temperature changes from −40 °C to 150 °C or even higher [9,10], driving IMC growth as a function of time and progressively converting ductile solder into brittle IMCs. This growth in solid-state is of particular technology concern, since it occurs continuously and may cause delayed and unpredictable problems.

The undercooling behaviour of Sn-rich Pb-free solders is also an issue, and the use of trace elements to reduce undercooling has been successful [11]. Previous research [11–14] suggests that the nucleation of β-Sn phases due to impurity elements, such as Zn, Co, and Fe reduces the undercooling of Sn-rich solder alloys. These various alloying elements also have major effects on solder/substrate reactions, as they are either soluble in the IMC layer (e.g., Ni, Au, Co, etc.), or form new interfacial IMC barrier layers (e.g., Fe, Al, P, etc.) [15]. Small additions of Zn into Pb-free solder have received much attention in comparison to the other alloying elements [8,14,16–19] because of: (i) significantly reduced undercooling, (ii) thinner and void-free IMCs at the interface. Despite the benefits of Zn, use of SAC + Zn solder alloy particles in the solder paste generally fails due to excessive oxidation of the particles resulting in incomplete particle coalescence during reflow. Other attempts to introduce Zn into the system during reflow of solder

* Corresponding author. Tel.: +44 0207 848 2370; fax: +44 0207 848 2932.
*E-mail address:* hiren.kotadia@kcl.ac.uk (H.R. Kotadia).

0925-8388/$ – see front matter © 2011 Elsevier B.V. All rights reserved.
doi:10.1016/j.jallcom.2011.09.024

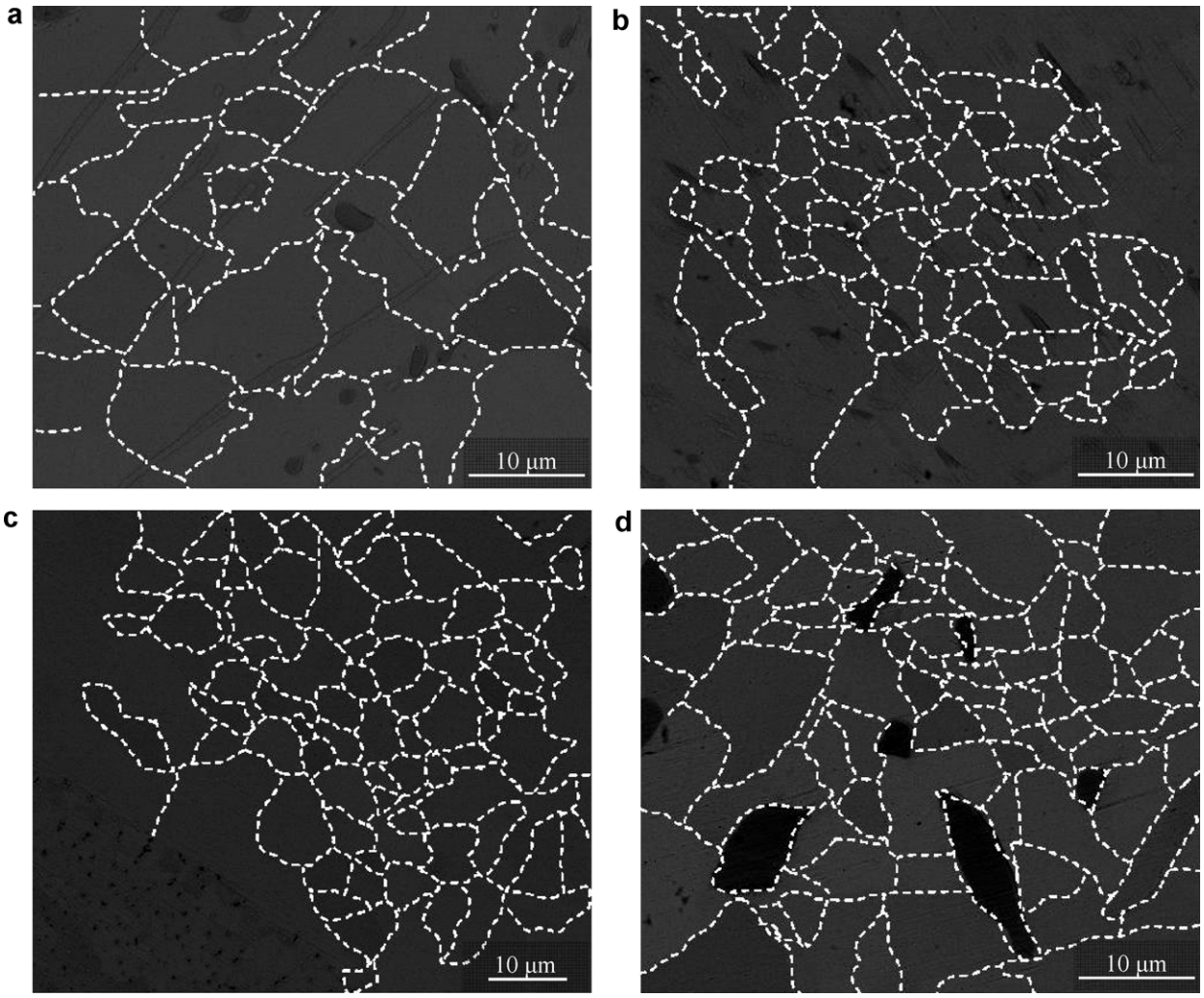


**Fig. 1.** SEM images showing the grain sizes in fabricated ingots of different solder alloys: (a) SAC, (b) SAC–0.5Zn, (c) SAC–1Zn, and (d) SAC–1.5Zn.

paste include the use of Cu–Zn substrates [20] and Zn compounds in the flux [21]. In this paper we extend the existing studies of IMC suppression to higher temperatures (150 °C and 185 °C) and increase understanding of the mechanism of IMC growth suppression. We also show that the mixing Zn particles in the 1–5 μm range into solder paste results in solder reflow and incorporation of Zn into the IMCs.

## 2. Experimental procedure

### 2.1. Alloy preparation

Sn–3.5Ag–0.7Cu (SAC) alloy was supplied by Henkel Ltd., UK. The SAC solder alloy with various amounts of Zn wt.% (0.5, 1, 1.5), subsequently referred to as SAC–0.5Zn, SAC–1Zn, and SAC–1.5Zn solder alloys, were fabricated in-house by dissolving the corresponding metallic foils at 420 °C for 20 min in a ceramic crucible using an electrical resistance furnace (all compositions in this article are given in weight percent unless otherwise stated). The fabricated ingot micrographs are shown in Fig. 1. There is no Zn segregation observed in any of the SAC–Zn solder ingots. Predetermined weights of solder were cut from the ingot and cleaned using acetone before soldering. The melting point and undercooling of solder alloys were measured by differential scanning calorimetry (DSC). The DSC experiment heating and cooling rate was fixed at 10 °C min$^{-1}$ range from 25 °C to 250 °C. The undercooling ($\Delta T$) is determined as the temperature difference between the melting point on the heating curve and the onset temperature of solidification on the cooling curve. DSC results are tabulated in Table 1.

### 2.2. Preparation of samples

Ni–P substrates were supplied by Schlumberger, Paris and consisted of Electroless Ni Immersion Gold (ENIG) bond pads on polyimide boards. The Cu substrates consisted of Cu coated FR4. The substrates were cut into 5 mm square plates with Cu thickness of 35 μm. Before reflowing, the substrate was cleaned using IPA (isopropyl alcohol), acetone and, finally, deionised water. For all of the alloys, 0.010 ± 0.003 g samples of solder alloy were cut from the solidified ingot, cleaned, coated by a thin layer of Henkel LF318 flux, and placed onto the substrate with a solder layer approximately 1.5 mm in maximum thickness and sent into a benchtop reflow oven (MRO

**Table 1**
Differential scanning calorimetry (DSC) test results for solder alloys.

| Alloy composition (wt.%) | Onset melting temperature during heating ($T_1$) (°C) | Onset solidification temperature during cooling ($T_2$) (°C) | Undercooling $\Delta T = T_1 - T_2$ (°C) |
|---|---|---|---|
| Sn-3.8Ag–0.7Cu | 217.73 | 199.89 | 17.84 |
| (Sn-3.8Ag–0.7Cu)–0.5Zn | 216.23 | 212.06 | 4.17 |
| (Sn-3.8Ag–0.7Cu)–1Zn | 216.65 | 212.61 | 4.04 |
| (Sn-3.8Ag–0.7Cu)–1.5Zn | 215.86 | 213.32 | 2.54 |

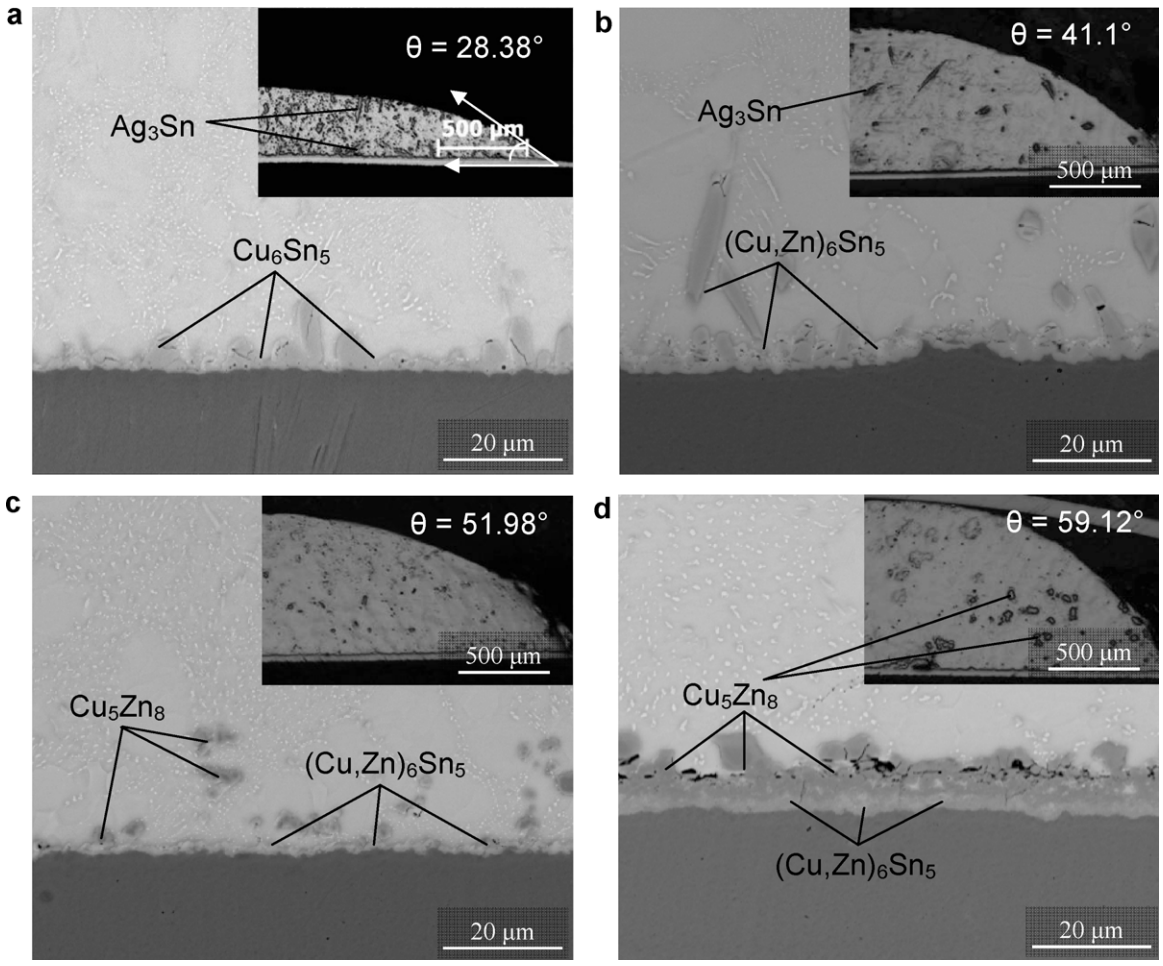


**Fig. 2.** SEM images showing the interfacial microstructures for different systems after reflow on Cu substrate: (a) SAC, (b) SAC–0.5Zn, (c) SAC–1Zn, and (d) SAC–1.5Zn. The inserts show low magnification optical images where $\theta$ represents the solder ball contact angle.

160). The reflow was carried out in air by preheating at 140 °C for 150 s and soldering at 260 °C for 60 s. The molten solder was then allowed to cooled to room temperature by natural convection in air and finally cleaned of flux residues using acetone. The resulting solder samples form a hemispherical cap with a maximum thickness of 1 mm at the top of the solder dome and the average thickness of solder is 0.54 mm. For the SAC and SAC–Zn solder alloys, high temperature storage of the samples was carried out in air at 150 °C and 185 °C for between 1 and 1000 h, as to reveal the IMC growth kinetics under solid-state reactions.

### 2.3. Solder paste preparation

While solder alloys prepared as described in Section 2.1 were used for the bulk of the IMC growth experiments, solder pastes mixed with Zn powder were also prepared. SAC alloy particles were supplied by Henkel (Sn–3.5Ag–0.7Cu particles of 20–38 μm diameter) and mixed with Zn powder and Henkel LF318 flux. The Zn powder (1–5 μm diameter) was supplied by Goodfellow, UK and the compositions were 86% metal in the paste and SAC–(0–1.5)Zn nominal alloy composition assuming all the added Zn is incorporated into the solder rather than expelled with the flux during reflow.

### 2.4. Microscopy and quantitative metallography

The reflowed and the thermally aged samples were prepared for observations of cross-sectional structure. The samples were cut perpendicular to the substrate using a diamond blade and polished with SiC abrasive papers and finally with 3 μm and 0.25 μm diamond suspensions. In order to quantify the IMC layer thickness 100 data points were taken for each solder–substrate combination. In order to obtain the top view of IMCs, the majority of the solder on the specimen was ground away, and then the specimens were etched with 17% concentrated nitric acid for approximately 30 min to selectively dissolve the remaining solder.

The microstructures of the samples were observed without etching under a ZEISS Axioscop2 MAT optical microscope equipped with an automated Zeiss AxioVision image analyser, which was used for the preliminary microstructural investigation and quantitative analysis. A FEI scanning electron microscope (SEM) equipped with energy-dispersive X-ray spectroscopy (EDX) at an accelerating volt-

**Table 2**
Elemental analysis of $(Cu,Zn)_6Sn_5$ and $(Cu,Ni,Zn)_6Sn_5$ interfacial IMCs by EDX, after reflow (0 h) and 1000 h storage at 150 °C.

| Alloys | | $(Cu,Zn)_6Sn_5$ at Cu substrate, wt.% (at.%) | | | $(Cu,Ni,Zn)_6Sn_5$ at Ni–P substrate, wt.% (at.%) | | | |
|---|---|---|---|---|---|---|---|---|
| | | Cu | Zn | Sn | Ni | Cu | Zn | Sn |
| (Sn-3.8Ag–0.7Cu)–0.5Zn | 0 h | 35.8 (50.9) | 0.2 (0.3) | 64.0 (48.8) | 12.4 (19.1) | 21.2 (30.2) | 0.4 (0.6) | 66.0 (50.1) |
| | 1000 h | 62.5 (74.5) | 3.2 (3.7) | 34.3 (21.8) | 16.7 (21.7) | 37.7 (45.5) | 6.5 (7.6) | 39.1 (25.2) |
| (Sn-3.8Ag–0.7Cu)–1Zn | 0 h | 38.3 (52.1) | 5.0 (6.6) | 56.7 (41.3) | 9.1 (14.5) | 19.4 (28.5) | 1.1 (1.6) | 70.4 (55.4) |
| | 1000 h | 70.0 (78.3) | 7.6 (8.3) | 22.4 (13.4) | 17.4 (22.9) | 32.8 (39.8) | 9.2 (10.8) | 40.6 (26.4) |
| (Sn-3.8Ag–0.7Cu)–1.5Zn | 0 h | 41.7 (54.7) | 7.2 (9.2) | 51.1 (36.1) | 31.9 (38.6) | 27.4 (30.6) | 13.3 (14.4) | 27.4 (16.4) |
| | 1000 h | 41.2 (55.5) | 3.3 (4.4) | 55.5 (40.1) | 26.0 (32.0) | 27.5 (31.2) | 17.1 (18.9) | 29.4 (17.9) |

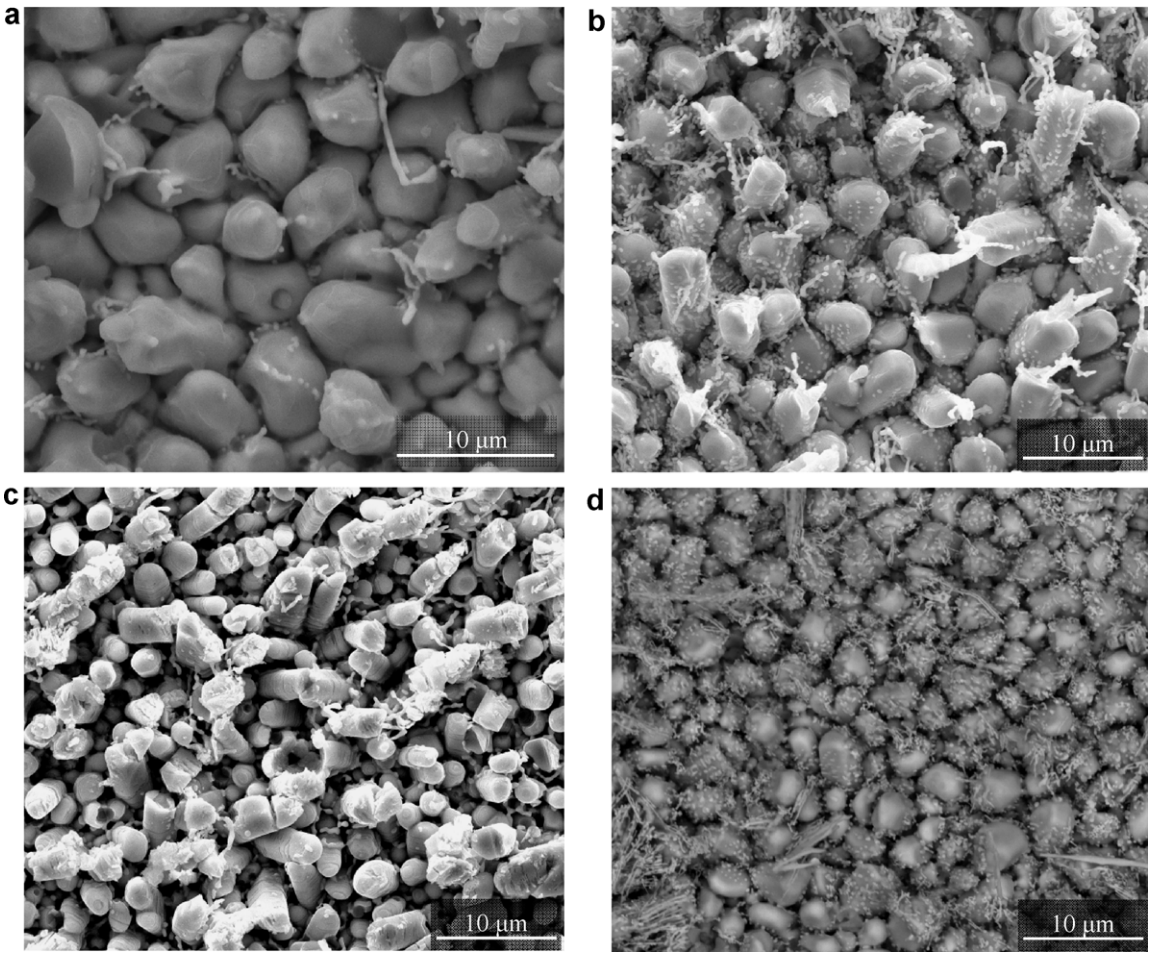


**Fig. 3.** Representative SEM images of $Cu_6Sn_5$ and/or $(Cu,Zn)_6Sn_5$ from top view for different systems: (a) SAC, (b) SAC–0.5Zn, (c) SAC–1Zn, and (d) SAC–1.5Zn, after reflow on Cu.

age of 10–25 kV was employed to achieve higher magnification in areas of interest, and to characterise the interfacial structures and compositions of the IMCs formed between the solder and substrate after reflow and during the high temperature storage.

The cumulative probability curves of the thicknesses of IMCs formed in the samples stored at 150 °C for 1000 h for different systems were plotted on normal probability coordinates, where the vertical axis represents the inverse of a cumulative Gaussian distribution, expressed as [22]:

$$\phi^{-1}[F(X)] = -\frac{\mu}{\sigma} + \frac{1}{\sigma}X \quad (1)$$

where $\mu$ is the mean, $\sigma$ is the standard deviation and $F(X)$ is the cumulative Gaussian function:

$$F(X) = \frac{1}{\sigma\sqrt{2\pi}} \int_{-\infty}^{X} \exp\left(\frac{X-\mu}{2\sigma^2}\right) dX \quad (2)$$

For data following an ideal normal distribution, the cumulative probability curve would be a straight line on the normal probability coordinates.

## 3. Results

### 3.1. Intermetallic compound growth between solder and Cu substrate

Fig. 2a is a typical cross-sectional SEM image and EDX analysis reveals (Table 2) the standard interfacial reaction and IMCs formed between SAC solder and Cu substrate during reflow. Cu diffuses rapidly into the molten solder and forms η-$Cu_6Sn_5$ scallop shaped IMC grains [5–7], while a much thinner ε-$Cu_3Sn$ IMC layer develops between the η-$Cu_6Sn_5$ and the Cu substrates. The $Cu_6Sn_5$ IMC forms at the substrate/solder interface because $Cu_6Sn_5$ has lower

**Table 3**
Different solder alloys on Cu substrate: observed IMCs, effective interdiffusion coefficient, $Ag_3Sn$ plate size, and contact angle.

| Alloys | Observed IMC | $D_{eff}$ | | Average size of $Ag_3Sn$ plates (μm) | Avg. contact angle (°) |
|---|---|---|---|---|---|
| | | $Cu_6Sn_5/(Cu,Zn)_6Sn_5$ ($cm^3\ s^{-1}$) | $Cu_3Sn$ ($cm^2\ s^{-1}$) | | |
| Sn–3.8Ag–0.7Cu | $Cu_6Sn_5$, $Cu_3Sn$ layer $Ag_3Sn$ plate | $8.39 \times 10^{-14}$ | $2.07 \times 10^{-14}$ | 84.2 | 28.38 |
| (Sn–3.8Ag–0.7Cu)–0.5Zn | $(Cu,Zn)_6Sn_5$, $Cu_3Sn$, and $Ag_3Sn$ plate | $3.98 \times 10^{-15}$ | | 60.3 | 41.10 |
| (Sn–3.8Ag–0.7Cu)–1Zn | $(Cu,Zn)_6Sn_5$, $Cu_3Sn$ layer, $Ag_3Sn$ plate and $Cu_5Zn_8$ particles | $8.61 \times 10^{-15}$ | | 54 | 51.92 |
| (Sn–3.8Ag–0.7Cu)–1.5Zn | $(Cu,Zn)_6Sn_5$, $Cu_3Sn$, $Cu_5Zn_8$ layer, $Ag_3Sn$ plate and $Cu_5Zn_8$ particles | $5.8 \times 10^{-15}$ | | 35.9 | 59.12 |

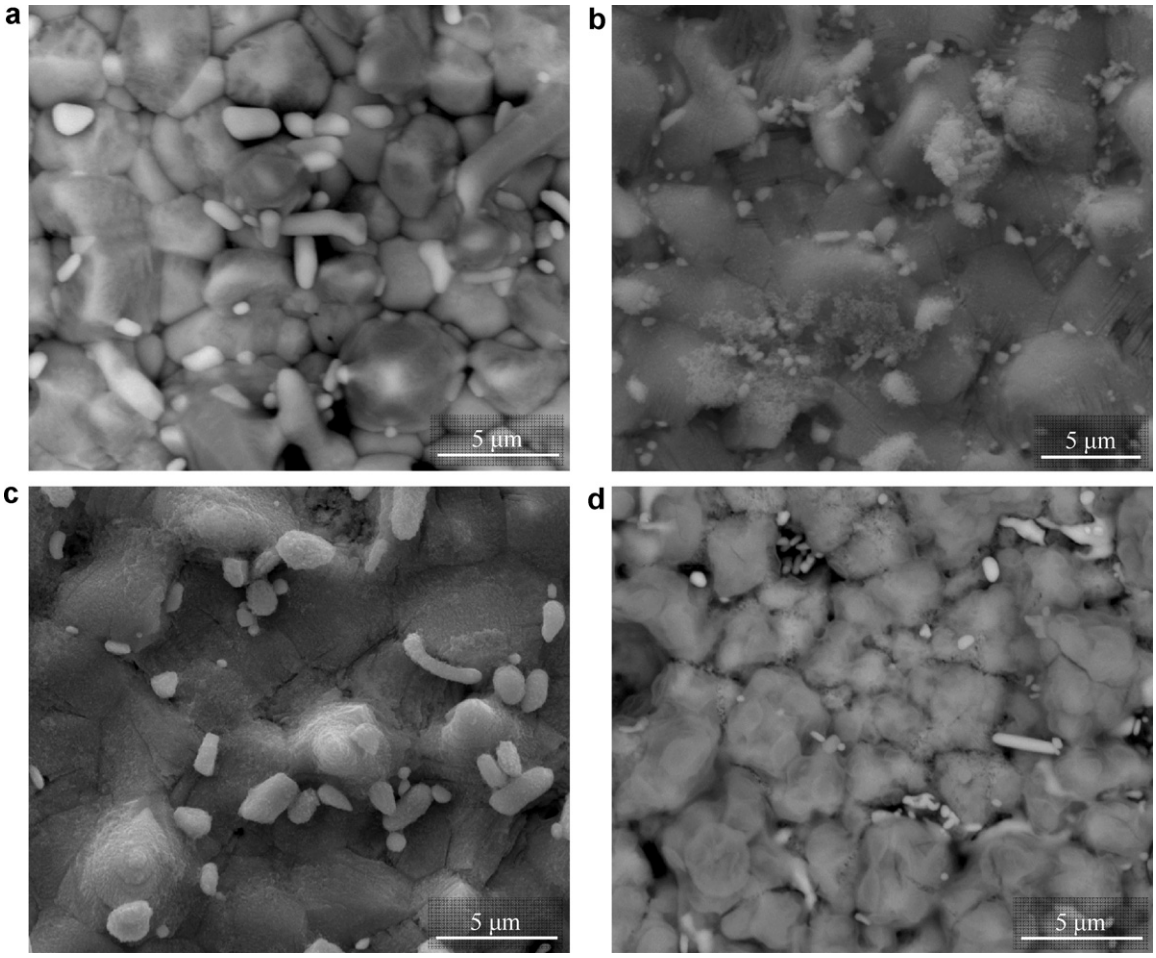


**Fig. 4.** Representative SEM images of $Cu_6Sn_5$ and/or $(Cu,Zn)_6Sn_5$ from top view for different systems: (a) SAC, (b) SAC–0.5Zn, (c) SAC–1Zn, and (d) SAC–1.5Zn, after 100 h of storage at 150 °C.

activation energy compared to the $Cu_3Sn$. However, the $Cu_6Sn_5$ IMC layer is thermodynamically unstable and therefore, $Cu_3Sn$ IMC will form over time by consuming the $Cu_6Sn_5$ IMC layer [7]. The solder/Cu system has a structure of Sn-rich grains (β-Sn) with some $Ag_3Sn$ plate and $Cu_6Sn_5$ phase precipitated above the interfacial IMC.

To understand the effects of Zn addition on the microstructure modification, careful observation and examination were carried out by the EDX analysis, which was used to detect any segregation of Zn atoms during interfacial reactions of the solder on Cu substrates. The IMCs formed on the interface and solder matrix strongly depend on the amount of Zn wt.% addition into the basic SAC solder alloy. Immediately after the reflow, 0.5–1 wt.% Zn addition modified the $Cu_6Sn_5$ IMC found in SAC/Cu couples to $(Cu,Zn)_6Sn_5$ (Fig. 2b and c) with the exact compositions given in Table 2. By contrast, the addition of 1.5 wt.% Zn resulted in Cu–Zn (i.e., γ-$Cu_5Zn_8$ [23]) IMC formation, followed by massive spalling of this layer into the solder (Fig. 2d). The phenomenon of massing spalling occurs when depletion of Zn in the solder due to formation of the $Cu_5Zn_8$ means that this reaction product is no longer in local thermodynamic equilibrium with the solder [24]. The $Cu_6Sn_5$ phase that is now in thermodynamic equilibrium replaces the $Cu_5Zn_8$ resulting in a 3 layer structure at the interface; $Cu_6Sn_5$ next to the Cu substrate, a 3–4 μm thick $Cu_5Zn_8$ layer in the solder and the gap between the two occupied by solder. It is important to note that massive spalling occurs due to the limited solder volumes in the system and does not occur when using a large volume solder bath (repeating the experiment in a solder bath resulted in the $Cu_5Zn_8$ layer remaining attached to the Cu substrate). In the SAC–1Zn and SAC–1.5Zn systems several IMCs containing Zn also precipitated in the solder matrix CuSnZn, $Cu_5Zn_8$, $AgZn_3$, $Ag_5Zn_8$ [25,26].

$Ag_3Sn$ IMC plate also forms during solidification due to the slow cooling rate, often nucleating and growing from the interfacial $Cu_6Sn_5$ layer, as seen in Fig. 2a (inset). These may have a detrimental effect on the solder reliability due to a weak interface between $Ag_3Sn$ and the tin matrix phase [12]. The number of large $Ag_3Sn$ plates in the SAC/Cu system was estimated by counting the $Ag_3Sn$ plates of length greater than the average of 84.2 μm. In contrast to the SAC/Cu system, the SAC–Zn/Cu systems had a reduced number of plates and these had reduced size (insets in Fig. 2 and Table 3). Similar results were noted earlier [12].

Fig. 3 shows the morphologies of $(Cu,Zn)_6Sn_5$ grains formed with different Zn concentrations from the top-view. Fig. 3a shows that the $Cu_6Sn_5$ grain appears as a typical round scallop-type grain, homogeneously distributed across the Cu surface. With the addition of Zn, the morphology of the $(Cu,Zn)_6Sn_5$ grains becomes in one case an elongated, rod-like shape (SAC–1.0Zn) but generally the number IMC grains per unit area are significantly higher than in the SAC–Zn/Cu system. The white spots on the surface of the $Cu_6Sn_5$ grains have previously been reported as $Ag_3Sn$ nanoparticles [27].

The IMCs formed after soldering continues to grow at the ageing temperature by interdiffusion between the elements of the solder and the Cu substrate, resulting in morphology changes and increased thickness. Fig. 4 shows that after 100 h storage at 150 °C,

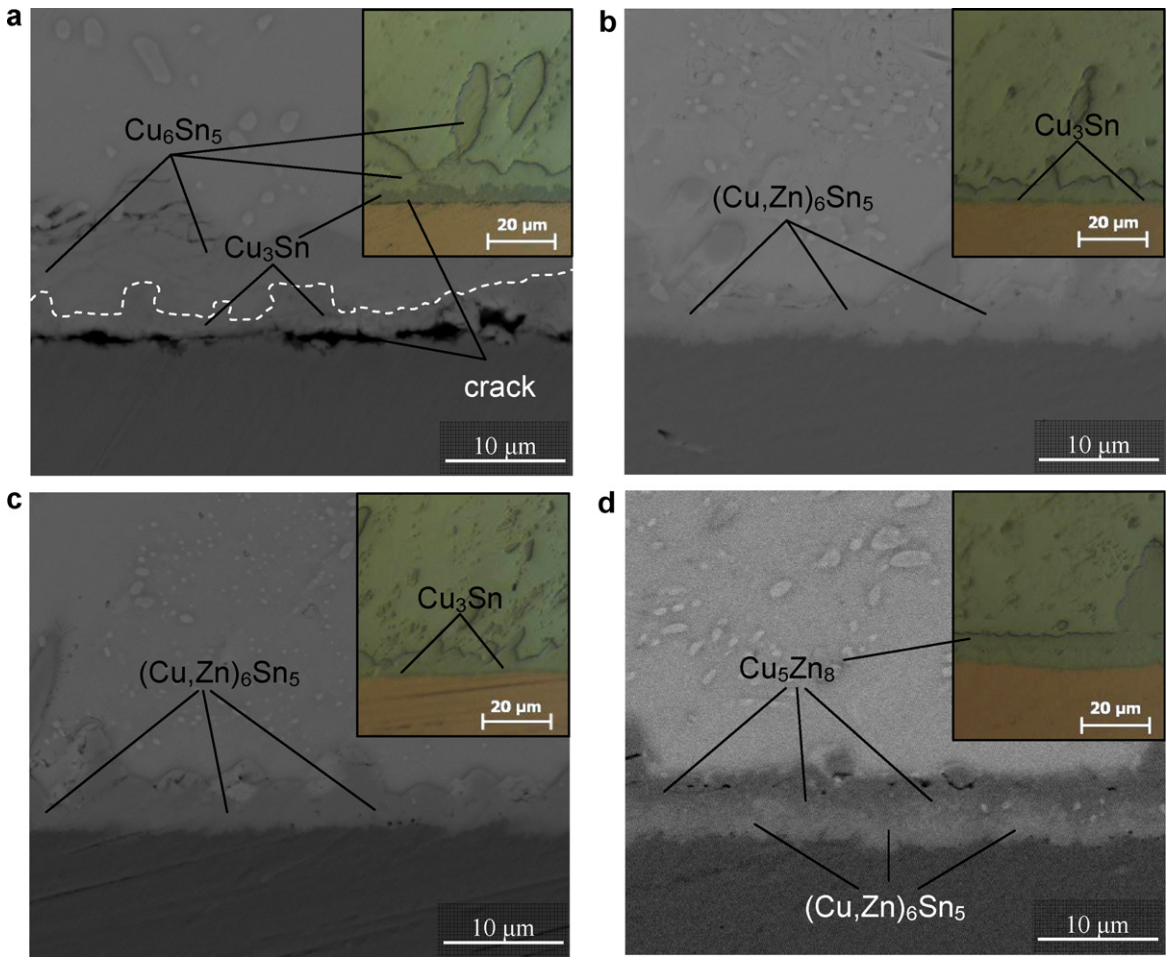


**Fig. 5.** SEM images showing IMC growth after 1000 h of storage at 150 °C on Cu substrate for different systems: (a) SAC, (b) SAC–0.5Zn, (c) SAC–1Zn, and (d) SAC–1.5Zn.

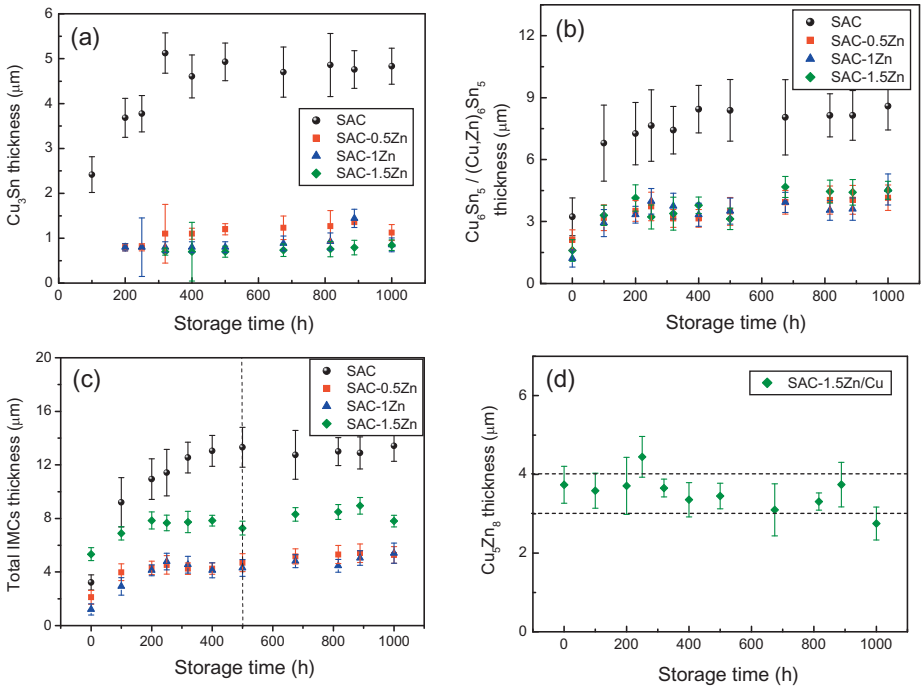


**Fig. 6.** Plots of mean IMC thickness versus storage time (a) thickness of $Cu_3Sn$ IMC layer, (b) thickness of $Cu_6Sn_5$ and $(Cu,Zn)_6Sn_5$ IMCs layer, (c) total IMC thickness, and (d) thickness of $Cu_5Zn_8$ IMC for the SAC–1.5Zn/Cu system, where the value corresponding to 0 h stands for the as-reflowed samples and the dotted line in figure (c) indicates the starting point of spalling of $Cu_6Sn_5$ IMC particles. All samples stored at 150 °C.

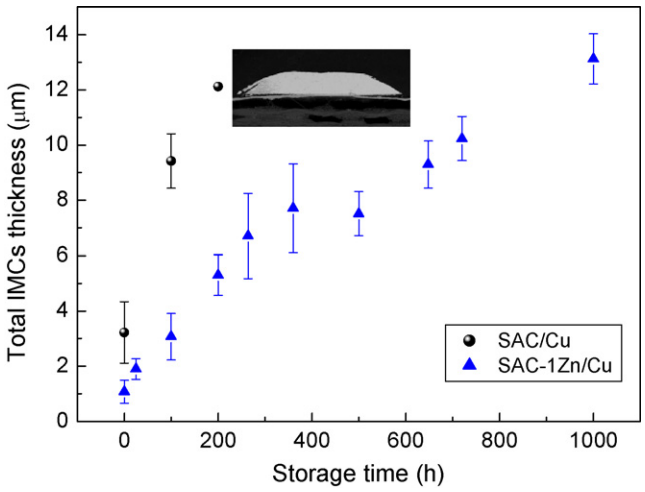


**Fig. 7.** Plots of mean IMC thickness versus storage time at 185 °C.

the channels between the $Cu_6Sn_5$ grains have narrowed considerably with the addition of Zn, especially in the SAC–0.5 and 1 wt.% Zn solder systems as compared with the SAC system.

Fig. 5 shows the growth of IMC layers after 1000 h storage at 150 °C. Elemental composition changes in the IMCs after are given in Table 2. The thickening kinetics of layers of $Cu_3Sn$, $(Cu,Zn)_6Sn_5$, and $Cu_5Zn_8$ are analysed by plotting the average thickness versus the storage time in Fig. 6. In the SAC/Cu system the $Cu_3Sn$ layer grows at the expense of $Cu_6Sn_5$ and the $Cu_6Sn_5$ IMC becomes smoother. In the SAC–Zn/Cu systems the $Cu_3Sn$ IMC layer appears after a delay of 200 h in high temperature storage. In these systems the $Cu_3Sn$ IMC layer only grew to about a maximum of 1 μm even after 1000 h (Figs. 6 and 7a). In the SAC/Cu system the $Cu_3Sn$ IMC layer becomes rougher (Fig. 5a) after high temperature ageing. In addition, numerous Kirkendall voids are observed at the $Cu_3Sn$/Cu interface but these appear to have been totally suppressed by the addition of Zn in the solder.

The suppression of the $Cu_3Sn$ and voids would be expected to improve the mechanical and electromigration reliability [14]. Evidence of this is seen in Fig. 5a, in which SAC solder has separated from the Cu substrate at 675 h. By contrast, these cracks do not occur in the SAC–Zn/Cu systems. In the SAC/Cu system after 500 h of storage, spalled $Cu_6Sn_5$ particles can be observed in the solder matrix, which is indicated by the dotted line in Fig. 6c; after this point the graph does not capture the true rate of IMC growth for the SAC/Cu system. After 1000 h the layer of solder between the $Cu_5Zn_8$ IMC and $Cu_6Sn_5$ IMC, has been almost entirely consumed by further growth of the $Cu_6Sn_5$ layer, visible in Fig. 5d. Small isolated pockets of solder remain at the interface between the two IMC layers, but the interface is otherwise almost completely planar, and the $Cu_5Zn_8$ IMC, therefore, acts as a barrier layer to further $Cu_6Sn_5$ layer growth. In particular, the $Cu_5Zn_8$ must act as a barrier layer to further diffusion of Sn in order to limit the thickness of the $Cu_6Sn_5$ layer. Further, the absence of $Cu_6Sn_5$ particles in the solder matrix shows that the $Cu_5Zn_8$ layer also blocks Cu diffusion in the other direction. $Cu_5Zn_8$ IMC thickness does not change with time (Fig. 6d).

The ageing results clearly demonstrate the total thickness of IMC significantly reduced from 13.5 μm (SAC) to ~3 μm (SAC–(0.5–1)Zn) on Cu substrate (Fig. 6c). It was found that the addition of 0.5–1 wt.% Zn into basic SAC solder alloy will be adequate to suppress Sn–Cu IMCs and that a higher amount of Zn into basic SAC solder alloy can only achieve slightly more IMC suppression and more Cu–Zn based IMCs particles into solder matrix. For that reason, high temperature storage at 185 °C was carried out on

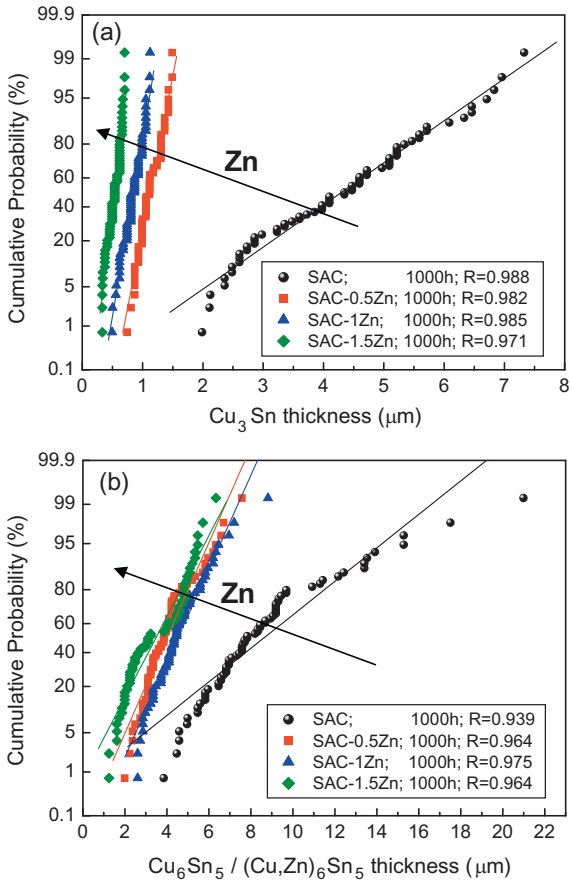


**Fig. 8.** Cumulative probability curves of the thickness of (a) $Cu_3Sn$ and (b) $Cu_6Sn_5$ or $(Cu,Zn)_6Sn_5$ formed on Cu substrate, stored at 150 °C for 1000 h on the normal coordinates.

only SAC and SAC–1Zn solder alloys. The measured IMC thickness with respect to the storage time is plotted in Fig. 7. The growth of IMCs in the SAC–1Zn/Cu system growth of IMCs is suppressed relative to the SAC/Cu system, but after 500 h an unacceptably thick IMC layer formed and numerous Kirkendall voids were observed close to the substrate. At the same time, in the SAC/Cu system cracks grew at the solder/substrate interface and at 200 h the solder has completely separated from the Cu substrate.

Fig. 8 shows cumulative probability curves of the IMCs thickness of Cu–Sn in the SAC/Cu and SAC–Zn/Cu samples with 1000 h storage time at 150 °C. In Fig. 8, the $R$ values quoted are the coefficients of correlation for a linear least squares fit between the data and a normal function. The closer the $R$ value is to 1.0, the closer the data fit to an ideal normal distribution. The fitted lines in Fig. 8 followed the normal distribution. Comparison of $R$ values showed that for most reaction conditions, the thickness of the $Cu_3Sn$ and $(Cu,Zn)_6Sn_5$ for SAC–(0.5–1.5)Zn/Cu samples appeared to follow the ideal normal distribution somewhat better than that of the SAC/Cu samples.

The wettability of solder alloy also changes with even a small amount of Zn addition into the basic SAC solder alloy (insets in Fig. 2 and Table 3). The surface energies of solder and substrate play an important role in determining wetting behaviour. This is mathematically described by classical Young's equation [28]:

$$\gamma_{GS} = \gamma_{LS} + \gamma_{GL} \cos \theta \quad (3)$$

where $\gamma_{GS}$, $\gamma_{LS}$, and $\gamma_{GL}$ refer to the surface tensions of the gas/surface, liquid/surface, and gas/liquid interface respectively and $\theta$ is the equilibrium contact angle. However, it is exceptionally difficult to measure $\gamma_{GS}$ and $\gamma_{GL}$ in Young's equation. The addition

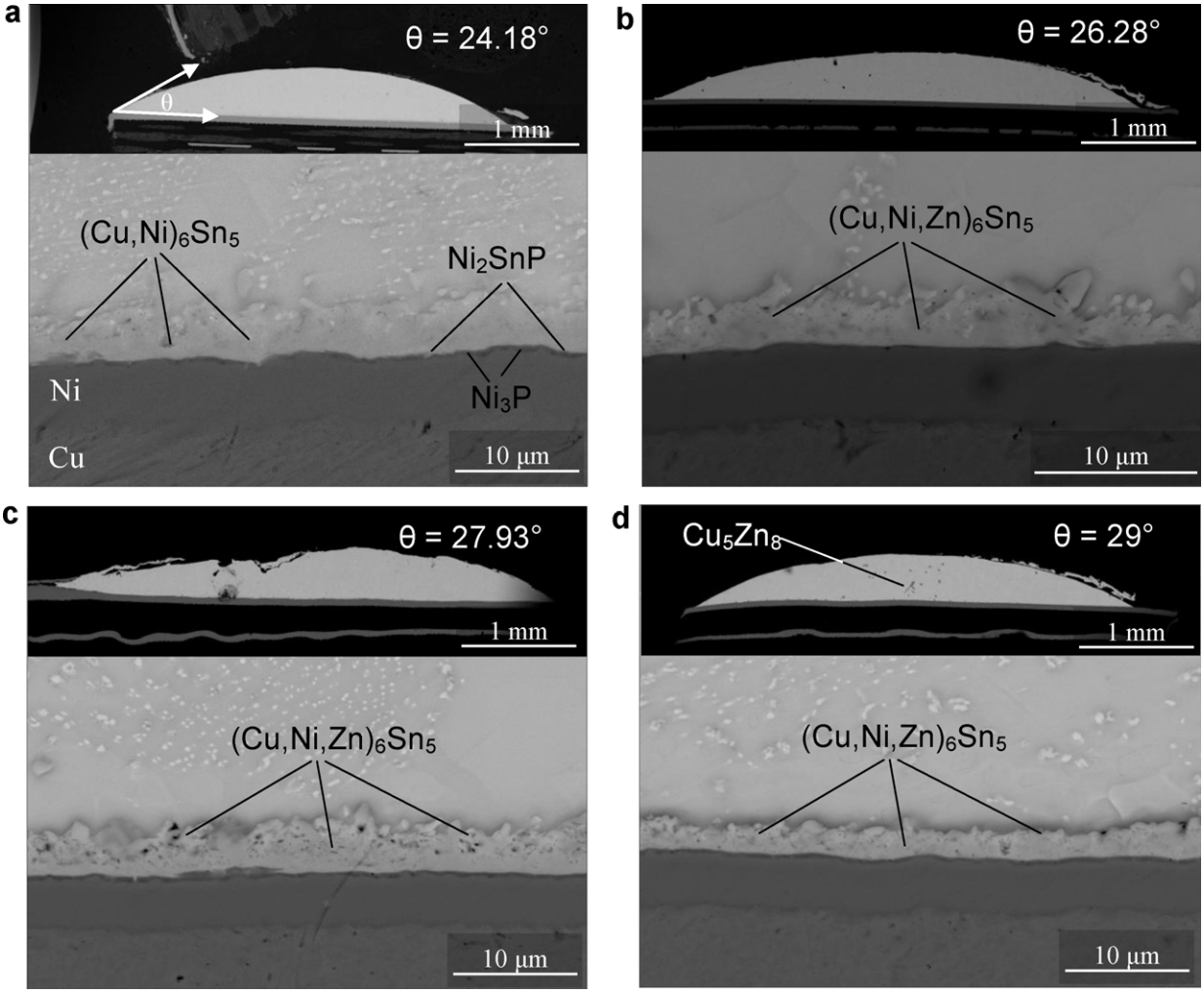


**Fig. 9.** SEM images showing the interfacial microstructures for different systems on Ni–P substrate: (a) SAC, (b) SAC–0.5Zn, (c) SAC–1Zn, and (d) SAC–1.5Zn. The inserts show low magnification SEM images where $\theta$ represents the solder ball contact angle.

of Zn progressively increases the measured contact angle from 28° (SAC) to 59° (SAC–1.5Zn), while even the SAC–0.5Zn system results in an angle of 41°. This increase has been attributed to oxidation of Zn atoms at the molten solder surface [29].

### 3.2. Intermetallic compound growth between solder and Ni–P substrate

The ENIG substrates will be referred to as Ni–P substrates subsequently as the Au top layer rapidly diffuses in the solder and plays no discernable role in subsequent solder–substrate interactions apart from one exception (see below). Fig. 9 shows a cross-section of the interface in a SAC/Ni–P system and SAC–(0.5–1.5)Zn/Ni–P systems. Three main IMCs: $Ni_3P$; $Ni_2SnP$ and $(Cu,Ni)_6Sn_5$ were observed in the SAC/Ni–P system, as depicted in Fig. 9a. The morphology of $(Cu,Ni)_6Sn_5$ IMC grains was needle-shaped while $Ni_3P$ and $Ni_2SnP$ IMCs formed as uniform layers. With the addition of Zn, it was found that the $(Cu,Ni)_6Sn_5$ IMC becomes $(Cu,Ni,Zn)_6Sn_5$. Other IMC's containing Zn are also observed in the solder matrix: $Cu_5Zn_8$ (Fig. 9d) and $Ni_5Zn_{21}$. As with the Cu substrate, the $Ag_3Sn$ IMC plate size significantly reduces with addition of Zn as noted in Table 3.

Fig. 10 shows that as the Zn concentration in the solder increases, the interfacial $(Cu,Ni,Zn)_6Sn_5$ IMC grains become progressively smaller. An additional feature in the SAC–1.5Zn/Ni–P system is the appearance of 15 μm size dendritic grains (composition: 17.45 at.% Ag, 6.11 at.% Sn, 6.11 at.% Ni, 35.77 at.% Cu, 27.35 at.% Zn, 7.22 at.% Au) embedded within the $(Cu,Ni,Zn)_6Sn_5$ layer (see inset in Fig. 10d). After 100 h storage at 150 °C, the $(Cu,Ni,Zn)_6Sn_5$ IMC grains form a layer type structure and the channel width between the grains reduces significantly as compared to the $(Cu,Ni)_6Sn_5$ IMC grains (see Fig. 11). The wetting angle with the substrate also increases with increasing Zn concentration in the solder although the effect is far less significant than with Cu substrate (Table 4).

The growth rate of the $(Cu,Ni,Zn)_6Sn_5$ IMC was slow compared to the IMC growth on Cu substrate, due to the limited supply of Cu, and slower release of Ni from the substrate. Fig. 12 shows cross-section SEM micrographs of the SAC/Ni–P and SAC–(0.5–1.5)Zn/Ni–P system aged at 150 °C for 1000 h. The presence of $Ni_5Zn_{21}$ IMC grains is also more visible at the interface after ageing. The concentration of Zn at the interface in all three solder alloys was measured and tabulated in Table 2. Fig. 13 shows the growth of interfacial IMC thickness with time. In the SAC–Zn solder alloy systems, interfacial IMC growth is clearly lower than with the SAC system with the lowest growth rate observed with the highest concentration of Zn. Thus while the $(Cu,Ni)_6Sn_5$ IMC layer grew to 8.5 μm after 1000 h storage at 150 °C in the SAC/Ni–P system, the equivalent thickness in the SAC–1.5Zn/Ni–P system is 2.5 μm. After ageing at 185 °C for 1000 h, $(Cu,Ni)_6Sn_5$ IMC grew to 12 μm thickness with SAC

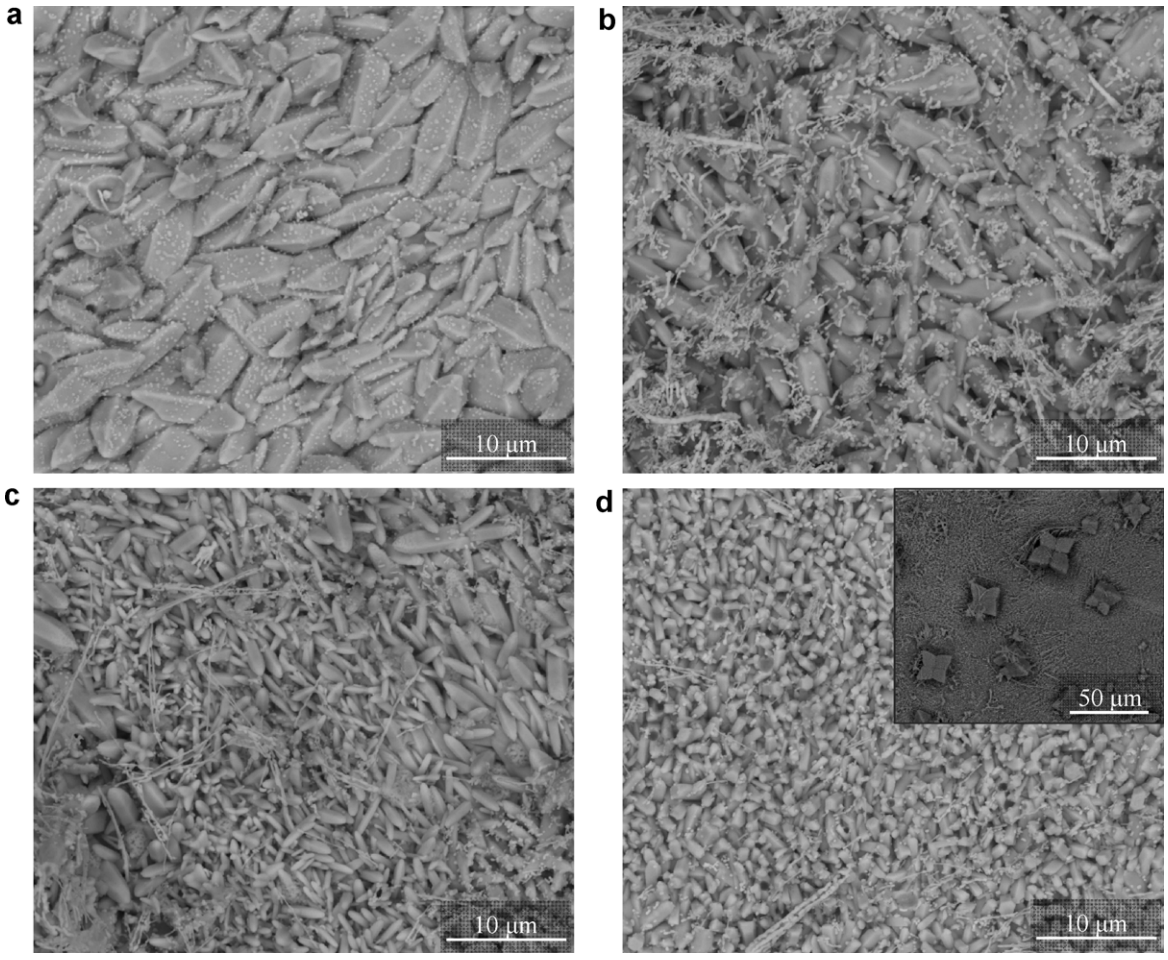


**Fig. 10.** Representative SEM images of $(Cu,Ni)_6Sn_5$ and/or $(Cu,Ni,Zn)_6Sn_5$ from top view for different systems: (a) SAC, (b) SAC–0.5Zn, (c)SAC–1Zn, and (d) SAC–1.5Zn (insert shows images of Ni–Cu–Sn–Zn–Au particles), after reflow.

solder, while $(Cu,Ni,Zn)_6Sn_5$ IMC grew to only 5 μm in the SAC–1Zn system. Additionally, at the SAC/Ni–P interface, Kirkendall voids were observed inside the $Ni_3P$ layer. The thicknesses of $(Cu,Ni)_6Sn_5$ and $(Cu,Ni,Zn)_6Sn_5$ IMC in the SAC/Ni–P and SAC–(0.5–1.5)Zn/Ni–P systems followed the normal distribution very well (Fig. 14), in a similar manner to the IMCs in the Cu substrate.

### 3.3. Solder Paste + Zn reflowed on Cu and Ni–P substrate

After the addition of Zn powder to solder paste the mixture was reflowed in a benchtop reflow oven. The following observations were made after cross sectioning and reflow: (i) The solder alloy particles coalesced as they would have in a normal solder paste, (ii) the wetting angle increased on Cu and Ni–P substrates in a similar manner to that observed in the SAC + Zn alloy experiments, (iii) some Zn particles were expelled along with the flux (see Fig. 15), (iv) the IMC compositions were similar to those observed in the corresponding SAC + Zn alloy experiments, and (v) the thickness of the IMC's was reduced slightly from the corresponding SAC + Zn alloy experiments by 22% suggesting that 78% of the Zn powder has been retained in the solder.

## 4. Discussion

### 4.1. The effect of Zn addition on bulk solder microstructure

Fig. 1 shows the formation of fine equiaxed primary β-Sn grains and Fig. 2 displays differences in β-Sn dendrite morphology and $Ag_3Sn$ IMC plates with the addition of a trace amount of Zn into the basic SAC solder alloy. It is well known that a solidification structure depends strongly on the alloy composition, solidification conditions, or the type of nucleating substrates present. Literature suggests that in the absence of a grain refiner (where constitutional super-cooling driven nucleation is important), big bang (also

**Table 4**
Different solder alloys on Ni–P substrate: observed IMCs, effective interdiffusion coefficient, $Ag_3Sn$ plate size, and contact angle.

| Alloys | Observed IMC | $(Cu,Ni)_6Sn_5/(Cu,Ni,Zn)_6Sn_5$, $D_{eff}$ ($cm^2s^{-1}$) | Average size of $Ag_3Sn$ plates (μm) | Avg. contact angle (°) |
|---|---|---|---|---|
| Sn–3.8Ag–0.7Cu | $(Cu,Ni)_6Sn_5$,$Ni_2SnP$,$Ni_3P$ layer; $Ag_3Sn$ plate | $4.84 \times 10^{-14}$ | 73 | 24.18 |
| (Sn–3.8Ag–0.7Cu)–0.5Zn | $(Cu,Ni,Zn)_6Sn_5$, $Ni_2SnP$, $Ni_3P$ layer; $Ag_3Sn$ plate | $5.20 \times 10^{-15}$ | 57 | 26.28 |
| (Sn–3.8Ag–0.7Cu)–1Zn | $(Cu,Ni,Zn)_6Sn_5$, $Ni_2SnP$, $Ni_3P$ layer; $Ag_3Sn$ plate, $Ni_5Zn_{21}$ and $Cu_5Zn_8$ particles | $4.36 \times 10^{-15}$ | 45 | 27.93 |
| (Sn–3.8Ag–0.7Cu)–1.5Zn | $(Cu,Ni,Zn)_6Sn_5$, $Ni_2SnP$, $Ni_3P$ layer; $Ag_3Sn$ plate; $Ni_5Zn_{21}$, $Cu_5Zn_8$ particles | $8.71 \times 10^{-15}$ | 23 | 29 |

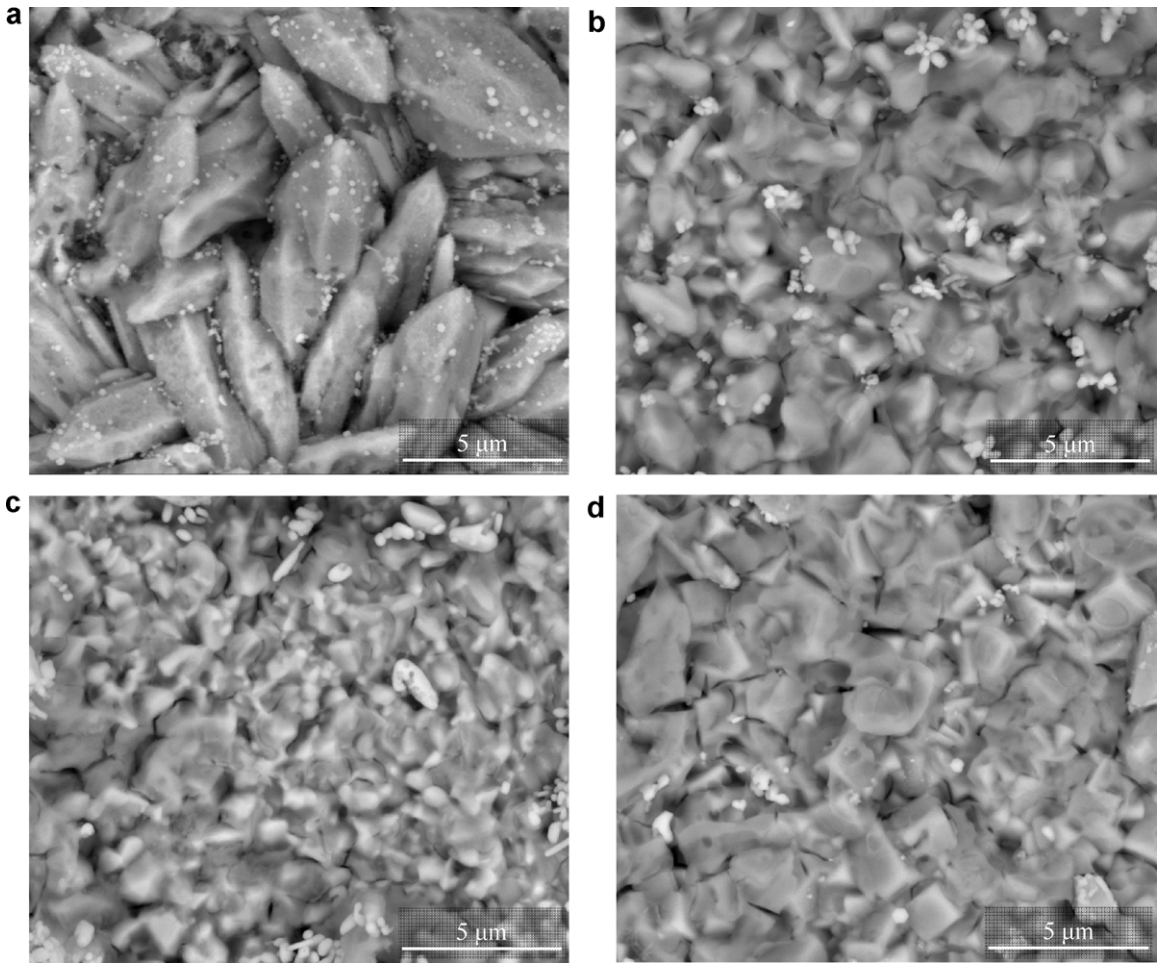


**Fig. 11.** Representative SEM images of $(Cu,Ni)_6Sn5$ and/or $(Cu,Ni,Zn)_6Sn_5$ from top view for different systems: (a) SAC, (b) SAC–0.5Zn, (c) SAC–1Zn, and (d) SAC–1.5Zn, after 100 h of storage at 150 °C on Ni–P substrate.

known as free chill crystal or wall mechanism), dendrite detachment mechanisms and solute atoms are the primary contributors to the creation of equiaxed or fine grains [30–32]. Alloy composition affects both the potency of nucleating particles through absorption at the liquid/particle interface and the efficiency through growth restriction by diffusion of solute in front of the solid/liquid interface at temperatures above the alloy liquidus temperature if this reduces the interfacial energy. This phenomenon can be explained by the growth restriction factor (GRF or *Q*) [33]. The GRF can be calculated as:

$$Q = \sum_{i=1}^{N} m_i C_{0i}(k_i - 1) \quad (4)$$

where *N* is the total number of solute elements in the alloy system, *i* represents the parameters of the *i*th element, and $k_i$, $m_i$, and $C_{0i}$ are the partition coefficient, the liquidus slope, and the initial composition of the *i*th element in the alloy, respectively. Soluble impurity elements (e.g., Zn) segregate at the advancing solid/liquid interface during the solidification and tend to slow the diffusion process, which prevents the grain growth, as has been demonstrated in Fig. 1. This constitutionally undercooled zone reduces the rate of grain growth and facilitates nucleation and the new grains do the same to the next grain, which results in a finer grain size in the solidified microstructure. There is less grain refining with 1.5 wt.% Zn than with 0.5 and 1 wt.% Zn. This could be due to the presence of Cu–Zn particles leading to the poisoning of grain refinement. The increasing nucleation by Zn solute effects in the liquid has a direct impact on the thermal history of the solidifying melt, as demonstrated by DSC results in Table 1. The primary β-Sn phase nucleation undercooling for SAC alloy is 18 °C, while Zn reduces under-cooling to about 4 °C. Additionally, reduction in undercooling also has a significant influence on $Ag_3Sn$ plate size by stopping nucleation of pro-eutectic $Ag_3Sn$ IMC plate and its extensive growth before the β-Sn phase nucleates in the solder. The experimental results shown in Fig. 2(inset) demonstrate this effect.

### *4.2. The morphologies of interfacial IMCs in the presence of liquid solder*

Significant differences were observed in interfacial IMC morphology upon addition of a trace amount of Zn into the solder (Figs. 3 and 10). The influence of Zn can be classed into two categories: (i) absorption of Zn atoms from the bulk solder into the $Cu_6Sn_5$ and $(Cu,Ni)_6Sn_5$ grains, and (ii) the presence of Zn in the molten SAC solder changes the interfacial energy between the molten solder and IMC grains, $\gamma_{Solder/Cu_6Sn_5}$ or $\gamma_{Solder/(Cu,Ni)_6Sn_5}$. It has been reported previously [34] that the $Cu_6Sn_5$ IMC grain morphology strongly depends on the interfacial energy between the molten solder and $Cu_6Sn_5$ IMC grains. At the substrate, the most stable interfacial IMC structure has the lowest interfacial energy. From thermodynamic considerations, higher $\gamma_{Solder/IMC}$ would promote the formation of semi-spherical IMC grains. Phase-field modelling studies show that lower $Cu_6Sn_5$/liquid interface energy is likely to create a more elongated type of morphology by increasing the

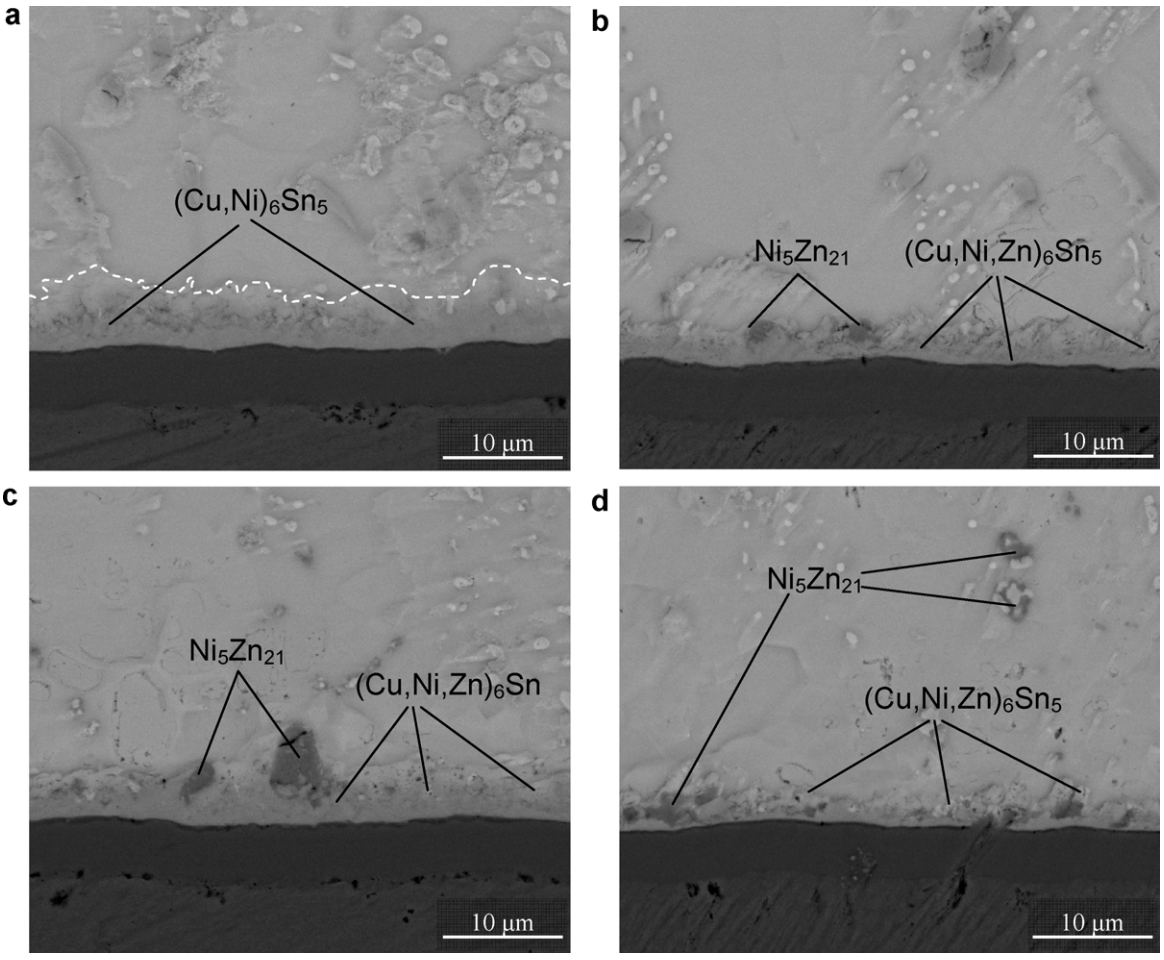


**Fig. 12.** SEM images showing IMC growth after 1000 h of storage at 150 °C on Ni–P substrate for different systems: (a) SAC, (b) SAC–0.5Zn, (c) SAC–1Zn, and (d) SAC–1.5Zn.

number of nuclei at the substrate and delaying grain coarsening [35] (e.g., Fig. 3c and 10d) while higher $Cu_6Sn_5$/liquid interface energy is likely to create a scallop-type morphology (e.g., Fig. 3a). Additionally, the low $\gamma_{Solder/IMC}$ would promote the growth of an irregular or facet morphology in the IMC compound grains.

Experimental [36] and theoretical work [35,37] show that the nucleation rate and growth of IMC grains can be controlled by the IMC/liquid interface energy. The Zn containing solder reduces the critical interfacial energy by the affinity between the Sn and Zn atoms.

### 4.3. The growth of interfacial IMCs during ageing

After the initial IMC's form at the interfaces by heterogeneous nucleation, further IMC growth depends on the diffusion mechanisms within the IMC layers. On Cu substrates, diffusion of Cu in the $Cu_6Sn_5$ IMC is likely to be faster than that of Sn because there is more Cu present (more excess vacancy sites) and the number of nearest neighbours is higher for the Cu atom than for a Sn atom [38]. Dyson et al. [39] concluded that at lower temperatures (below 150 °C), Cu interstitial diffusion is likely to be dominant, while at higher temperatures, Sn vacancy diffusion is preferred. Thus, in our study, Cu diffusion may have made a more important contribution to IMC growth at 150 °C, while Sn diffusion plays a stronger role at 185 °C.

However, during solid state ageing the IMC grain boundary or channel is the favoured diffusion path for IMC layer growth [7]. Therefore, the area percentage of grain boundary and grain morphology play a crucial role in determining IMC growth behaviour. The experimental results after 100 h storage at 150 °C reveal that area percentage of grain boundary in the solders containing Zn significantly decreased (Fig. 5b and c) lowering mass flux through the channels compared to the pure SAC solder. The growth of $Cu_3Sn$ at the Cu/$(Cu,Zn)_6Sn_5$ interface also appears to have been suppressed due to the lack of transport channels through the $(Cu,Zn)_6Sn_5$ layer.

On Ni–P substrate, with presence of Cu in the SAC solder, the formation of $Ni_3Sn_4$ is suppressed and instead $(Cu,Ni)_6Sn_5$ IMC forms. In fact, from Table 2, the Sn content in the IMC is seen to be 50 at.% initially, intermediate between the 57% expected in $(Ni,Cu)_3Sn_4$ and the 45% expected for $(Cu,Ni)_6Sn_5$. The high Cu content of 30 at.% far exceeds the 8.5% reported to be the limit that can be dissolved in $(Ni,Cu)_3Sn_4$ [40] confirming the identification of the IMC layer as $(Cu,Ni)_6Sn_5$. The addition of Zn to the SAC solder reduces interfacial IMC growth during high temperature ageing by reduction in the size and number of channels between the IMC grains in a similar manner to that observed on the Cu substrate (Fig. 11). With extended high temperature storage, Zn continuously accumulates at the interfacial IMC, forming a $(Cu,Zn)_6Sn_5$ or $((Cu,Ni,Zn)_6Sn_5$ IMC layer with higher Zn concentration, as noted in Table 2.

Figs. 7, 8 and 14 represent the IMC growth rates over time. The data has been fitted to a power law dependency on time as follows:

$$\Delta x - x_0 = (D_{eff}t)^n \quad (5)$$

where $\Delta x$ is the thickness of the IMC layer at ageing time $t$, $x_0$ is the IMC mean thickness immediately after reflow, $D_{eff}$ is the

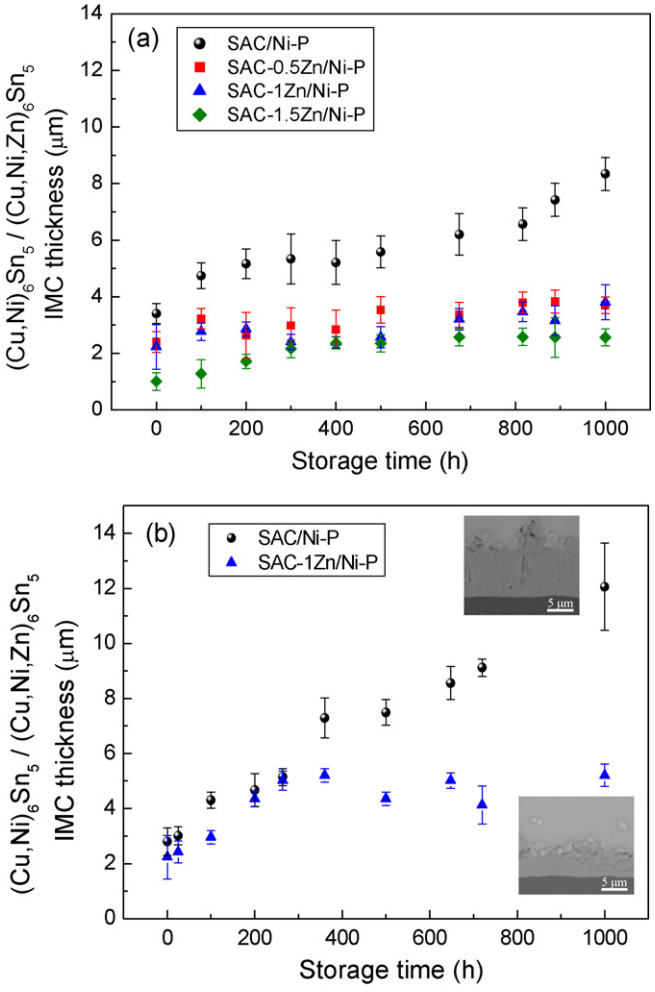


**Fig. 13.** Plots of mean IMC thickness versus storage time for different systems: (a) stored at 150 °C and (b) stored at 185 °C.

effective interdiffusion coefficient in the IMC layer, and $n$ is the time exponent. The values of $D_{eff}$ and $n$, for a particular ageing temperature, can be obtained by means of multivariable linear regression analysis. In our study, a linear regression analysis of the average thickness of the interfacial IMCs layer as a function of thermal

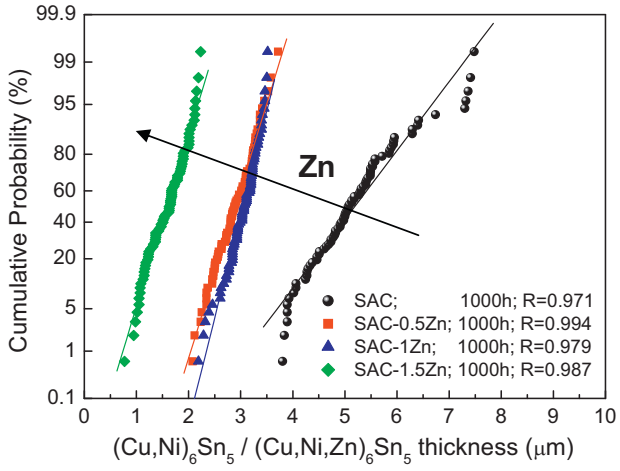


**Fig. 14.** Cumulative probability curves of the thickness of $(Cu,Ni)_6Sn_5$ and/or $(Cu,Ni,Zn)_6Sn_5$ formed on Ni–P substrate, stored at 150 °C for 1000 h on the normal coordinates.

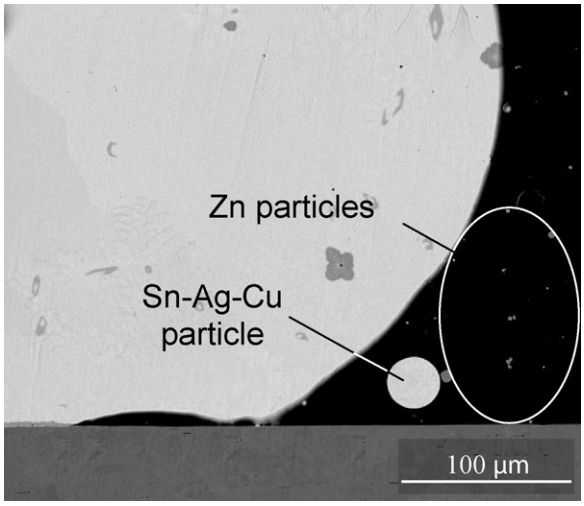


**Fig. 15.** SEM images of SAC–1.5Zn/Cu system prepared using SAC and Zn powders, showing expelled Zn particles in the flux.

ageing time was conducted to determine the best-fit $n$ values for the 150 °C ageing temperatures.

The calculated value of $n$ for $Cu_6Sn_5$ and $Cu_3Sn$ IMC was between 0.27–0.36 (~0.33) and 0.43 (~0.5) respectively and for $(Cu,Ni,Zn)_6Sn_5$ the $n$ value was between 0.49 and 0.57 (~0.5), using data taken from Figs. 6 and 13a. Some few data points which were affected by spalling were omitted from the analysis. When the exponent, $n$ is approximately 0.5, growth can attribute to the ideal diffusion-controlled model, and when $n$ approximately 0.33, growth is can attribute to the grain-boundary diffusion-controlled model. The $n$ value was used to calculate $D_{eff}$ and listed in Tables 3 and 4. In this study, the IMC $D_{eff}$ value was found to follow the order of $Cu_6Sn_5 > (Cu,Ni)_6Sn_5 > Cu_3Sn$. However, all three SAC–(0.5–1.5)Zn systems samples under most reaction conditions show significantly lower $D_{eff}$ values than their SAC counterparts.

In the case of 1.5 wt.% Zn containing solder, during the liquid-state reaction $Cu_5Zn_8$ IMC nucleates at the Cu substrate. As $Cu_5Zn_8$ IMC grows with time the Zn becomes depleted from the solder and local equilibrium at the interface shifts from the (Sn) + $Cu_5Zn_8$ two phase field to the (Sn) + $Cu_6Sn_5$ two phase field (which is more thermodynamically stable) [23]. Experimental results demonstrated that the $Cu_5Zn_8$ IMC layer acts as a barrier layer for Sn diffusion when the sample is stored at high temperature (Fig. 5d). Similar massive spalling phenomena is observed in other solder systems [14,24].

On Ni–P substrate $Ni_5Zn_{21}$ interfacial IMC phase was seen during ageing. Wang and Chen [19] studied the Sn/Ni–P system with various Zn concentrations; and the results showed that the various Zn concentrations would affect the reaction product species. The Sn–9 wt.% Zn or Sn–5 wt.% Zn solder would produce a relatively high-Zn-containing phase at interface, i.e., $Ni_5Zn_{21}$ and lower-Zn contain solder produce $(Ni,Zn)_3Sn_4$ phase at interface. Hence the formation of the $Ni_5Zn_{21}$ IMC is indicative of increasing Zn aggregation at the interface.

## 5. Summary and conclusions

Based on the experimental results the following conclusions can be drawn:

(i) In the SAC–Zn/Cu system immediately after reflow interfacial IMC thickness is reduced compared to the SAC/Cu system. For 0.5–1 wt.% Zn concentration the interfacial IMC is $(Cu,Zn)_6Sn_5$. When the Zn concentration is 1.5 wt.% a

$Cu_5Zn_8$ IMC layer forms followed by massive spalling leaving the more thermodynamically stable $Cu_6Sn_5$ IMC to form at the Cu/solder interface. Zn-containing IMCs such as CuSnZn, $Cu_5Zn_8$, $AgZn_3$, $Ag_5Zn_8$ IMC particles were observed in the solder matrix when the solder has more than 1 wt.% Zn concentration.

(ii) During high temperature ageing at 150 °C, in the SAC–(0.5–1.5)Zn/Cu system, $(Cu,Zn)_6Sn_5$ and $Cu_3Sn$ IMCs layers were suppressed significantly with Zn addition. The $Cu_5Zn_8$ IMC layer in SAC–1.5Zn/Cu system does not show any changes with ageing time. However, the spalled $Cu_5Zn_8$ IMC layer acts as a barrier layer for $Cu_6Sn_5$ interfacial IMC by stopping further diffusion of Sn from solder and Cu from substrate, limiting the $Cu_6Sn_5$ layer thickness during high-temperature storage.

(iii) On Ni–P substrate SAC–Zn solder alloy forms $(Cu,Ni,Zn)_6Sn_5$ IMC instead of $(Cu,Ni)_6Sn_5$. The higher Zn concentration solder alloys also showed $Ni_5Zn_{21}$ IMC grains close to the interface and Ni–Cu–Sn–Zn–Au particles embedded into interfacial IMC. At 150 °C, the $(Cu,Ni,Zn)_6Sn_5$ IMC layer grows with ageing time but the growth rate on Ni–P substrate is significantly lower than on Cu substrate. The lowest growth rate being found in the SAC–1.5Zn/Ni system.

(iv) At 185 °C ageing, addition of 1 wt.% Zn solder is able to suppress IMC growth on Ni–P substrate but on Cu substrate after 500 h an unacceptably thick IMC layer forms.

(v) On both Cu and Ni–P substrates the addition of Zn changes the $Cu_6Sn_5$ or $(Cu,Ni)_6Sn_5$ IMC morphology observed with SAC solders. While the initial grains formed after reflow are smaller and have a higher grain density, after 100 h of ageing at 150 °C the channels between the grains appear to be significantly reduced compared to the SAC solder and this may contribute to the slower subsequent growth rate.

(vi) The growth of the primary Sn-rich dendritic phase is restricted by the solute at the solid/liquid interface during solidification and $Ag_3Sn$ plate size is also significantly refined by reducing undercooling.

(vii) On Cu substrate the wetting angle increases by approximately 10° for every 0.5% increment in Zn concentration. On Ni–P substrate the increase is only 1.5°.

(viii) Zn powder based solder paste shows results similar to the SAC + Zn alloy experiments, but 22% of the added Zn was expelled along with the flux during reflow.

We conclude that 0.5–1 wt.% Zn addition is sufficient to limit the thickness of the interfacial IMCs for high temperature applications. More than 1 wt.% Zn solder leads to nucleation of excess Cu–Zn and Cu–Ni IMCs at the interface and poorer wetting, particularly on Cu substrates.

## Acknowledgments

This research was funded by the Engineering and Physical Sciences Research Council (Grant no. EP/G054339/1) in collaboration with Henkel Technologies, Dynex Semiconductor, and Schlumberger.

## References

[1] J.Y. Huh, K.K. Hong, Y.B. Kim, K.T. Kim, J. Electron. Mater. 33 (2004) 1161–1170.
[2] D.R. Frear, J.W. Jang, J.K. Lin, C. Zhang, JOM 53 (2001) 28–32.
[3] J. Glazer, Int. Mater. Rev. 40 (1995) 65–93.
[4] M. Abtew, G. Selvaduray, Mater. Sci. Eng. R 27 (2000) 95–141.
[5] K.N. Tu, K. Zeng, Mater. Sci. Eng. R 34 (2001) 1–58.
[6] T. Laurila, V. Vuorinen, J.K. Kivilahti, Mater. Sci. Eng. R 49 (2005) 1–60.
[7] K.N. Tu, Solder Joint Technology: Material, Properties, and Reliability, Springer, NY, USA, 2007.
[8] M.G. Cho, S.K. Kang, D. Shih, H.M. Le, J. Electron. Mater. 36 (2007) 1501–1509.
[9] S.H. Mannan, M.P. Clode, IEEE Trans. Adv. Pack. 27 (2004) 508–514.
[10] J.F. Li, S.H. Mannan, M.P. Clode, C. Johnston, A. Crossley, Acta Mater. 55 (2007) 5057–5071.
[11] M.G. Cho, H.Y. Kim, S. Seo, H.M. Lee, Appl. Phys. Lett. 95 (2009) 021905.
[12] S.K. Kang, D. Shih, D. Leonard, D.W. Henderson, T. Gosselin, S. Cho, J. Yu, W.K. Choi, JOM 56 (2004) 34–38.
[13] D.H. Kim, M.G. Cho, S. Seo, H.M. Lee, J. Electron. Mater. 38 (2009) 39–45.
[14] H.R. Kotadia, O. Mokhtari, M. Bottrill, M.P. Clode, M.A. Green, S.H. Mannan, J. Electron. Mater. 39 (2010) 2720–2731.
[15] T. Laurila, V. Vuorinen, M. Paulasto-Kröckel, Mater. Sci. Eng. R 68 (2010) 1–38.
[16] F. Wang, X. Ma, Y. Qian, Scripta Mater. 53 (2005) 699–702.
[17] M.G. Cho, S.K. Kang, S. Seo, D. Shih, H.M. Lee, J. Electron. Mater. 38 (2009) 2242–2250.
[18] F. Wang, F. Gao, X. Ma, Y. Qian, J. Electron. Mater. 35 (2006) 1818–1824.
[19] C. Wang, H. Chen, J. Electron. Mater. 39 (2010) 2375–2381.
[20] Y.M. Kim, H. Roh, S. Kim, Y. Kim, J. Electron. Mater. 39 (2010) 2504–2512.
[21] H. Sakuri, A. Baated, K. Lee, S. Kim, K. Kim, Y. Kukimoto, S. Kumamoto, K. Suganuma, J. Electron. Mater. 39 (2010) 2598–2604.
[22] J.F. Li, S.H. Mannan, M.P. Clode, D.C. Whalley, D.A. Hutt, Acta Mater. 54 (2006) 2907–2922.
[23] C. Chou, S. Chen, Acta Mater. 54 (2006) 2393–2400.
[24] S.C. Yang, C.E. Ho, C.W. Chang, C.R. Kao, J. Appl. Phys. 101 (2007) 084911.
[25] Y.K. Jee, Y.H. Ko, J. Yu, J. Mater. Res. 22 (2007) 1879–1887.
[26] J.M. Song, K.L. Lin, J. Mater. Res. 18 (2003) 2060–2067.
[27] X. Liu, M. Huang, Y. Zhao, C.M.L. Wu, L. Wang, J. Alloys Compd. 492 (2010) 433–438.
[28] T. Young, Philos. Trans. R. Soc. Lond. 95 (1805) 65–87.
[29] L.C. Prasad, A. Mikula, Physica B 373 (2006) 142–149.
[30] J. Hutt, D. StJohn, Int. J. Cast. Met. Res. 11 (1998) 13–23.
[31] S.C. Flood, J.D. Hunt, ASM Handbook, vol. 15, ASM, Materials Park, 1998, p. 170.
[32] A. Das, G. Liu, Z. Fan, Mater. Sci. Eng. A 419 (2006) 349–356.
[33] I. Maxwell, A. Hellawell, Acta Metall. 23 (1975) 229–237.
[34] S.J. Wang, C.Y. Liu, Acta Mater. 55 (2007) 3327–3335.
[35] M.S. Park, R. Arróyave, Acta Mater. 58 (2010) 4900–4910.
[36] H. Zhang, X.Y. Wang, L.L. Zheng, S. Sampath, Int. J. Heat Mass Transfer 47 (2004) 2191–2203.
[37] J.D. Robson, Acta Mater. 52 (2004) 4669–4676.
[38] X. Deng, G. Piotrowski, J.J. Williams, N. Chawla, J. Electron. Mater. 32 (2003) 1403–1413.
[39] B.F. Dyson, T.R. Anthony, D. Turnbull, J. Appl. Phys. 38 (1967) 3408, doi:10.1063/1.1710127.
[40] P. Sun, C. Andersson, X. Wei, Z. Cheng, D. Shangguan, J. Liu, J. Alloys Compd. 425 (2006) 191–199.